Persistent photoconductivity and photoionization of deep electron traps in Ga-doped $Cd_{1-x}Mn_xTe$

N. G. Semaltianos, G. Karczewski,* T. Wojtowicz,* and J. K. Furdyna
Department of Physics, University of Notre Dame, Notre Dame, Indiana 46556
(Received 3 September 1992)

Strong persistent photoconductivity (PPC) has been observed in bulk n-type $Cd_{1-x}Mn_xTe$ ($x=0.03$) crystals heavily doped with Ga at low temperatures (below ~ 150 K). The kinetics of the PPC effect were investigated by means of photoconductivity and photo-Hall measurements. The observed photoconductivity transients displayed a strongly nonexponential behavior. We use the observed transient behavior to show that the transfer of electrons from the ground state of defects, responsible for the PPC, to the conduction band proceeds in two steps, via an intermediate state of the defects. Numerical simulations based on the two-step photoionization model are in excellent agreement with the experimental data. From a detailed analysis of the spectral and temperature dependence of the carrier-concentration transients and of the photo-Hall data, we establish that the transition from the ground to the intermediate state is not accompanied by electron emission, i.e., the defect remains in the same charge state. The analysis of the spectral and temperature dependence of the photoionization cross sections indicates that both states of the defect are strongly coupled to lattice vibrations, and the large lattice relaxation mechanism is recognized as the mechanism responsible for the metastability of the free carriers leading to the observed PPC. In order to check whether the exchange interaction between magnetic Mn^{2+} ions and free electrons affects the photoionization process in $Cd_{1-x}Mn_xTe$, the photoconductivity transient measurements were repeated in the presence of magnetic fields up to $B=6$ T. No magnetic-field effect on photoemission has been observed, indicating that effects associated with deep levels are insensitive to the above exchange interaction.

I. INTRODUCTION

Persistent photoconductivity (PPC) is a property exhibited by certain semiconductors, where the exposure of the material to light at sufficiently low temperatures results in an increase of the carrier concentration that persists for a very long time (of the order of minutes to years) *after* the illumination is terminated. PPC has been observed in a large number of bulk semiconductors as well as in two-dimensional systems, and is one of the most interesting—although still not well understood—phenomena in contemporary semiconductor physics.

Through the years many mechanisms have been proposed to explain the origin of PPC, but only two major interpretations have survived successive confrontations with experimental data. The first of these is based on the existence of *macroscopic potential barriers* in semiconductors. Such potential barriers are expected to be present at surfaces, interfaces, and around doping or composition inhomogeneities. The presence of these macroscopic imperfections in the material creates built-in local electric fields that spatially separate the photogenerated electrons and holes and significantly decrease the recombination rate. The validity of this model was demonstrated in numerous instances. One of the most direct demonstrations was provided by Queisser and Theodorou,[1,2] who observed the PPC in selectively doped layered GaAs structures, where the potential barriers occur at the interfaces between the layers. The macroscopic barrier model is particularly suitable for describing PPC in artificially constructed semiconductor structures, such as the one just mentioned.

The second mechanism for generating PPC assumes the presence of *microscopic potential barriers,* which occur around certain defect centers as a result of emission of carriers trapped at the defect sites. At low temperatures these microscopic barriers prevent the carriers from being recaptured. The most common origin of such microscopic barriers is the relaxation of the crystal lattice around the defect. This mechanism, known as the large lattice relaxation (LLR) model, was proposed by Lang, Logan, and Jaros.[3,4] By assuming a strong coupling between the electronic and the vibrational properties of the defect centers, the LLR model readily explains most of the experimentally observed properties of the defects responsible for PPC. In particular, it accounts for the extremely small thermally activated electron-capture cross section and the very large Stokes shift of the ionization energy which characterizes such defects. The best known defects which lead to PPC due to the large lattice relaxation are the so-called *DX* centers observed and extensively investigated in $Al_xGa_{1-x}As$ and in GaAs (under hydrostatic pressure).[5] According to the widely accepted model of *DX* centers developed by Chadi and Chang,[6,7] the microscopic barrier and the defect center responsible for PPC arise from the interstitial-to-substitutional motion of the defect, triggered by the photoionization of an electron trapped at the defect.

In this paper we study PPC in the n-type semiconductor alloy $Cd_{0.97}Mn_{0.03}Te$ doped with Ga donors. This

material belongs to the group of semiconducting compounds referred to as diluted magnetic semiconductors (DMS's),[8] whose lattice is made up in part of substitutional paramagnetic Mn^{2+} ions. Because of the exchange interaction between the band electrons and the localized Mn^{2+} ions, DMS's exhibit interesting electronic properties in the presence of an external magnetic field, which are quite different from those of the "parent" nonmagnetic compound (in our case, CdTe). In the absence of a magnetic field, on the other hand, the net exchange interaction averages to zero and the band structure of $Cd_{1-x}Mn_xTe$, as well as its electrical and optical properties, are remarkably similar to those of pure CdTe. Because of its strong PPC effect—which in effect permits one to vary the electron concentration by dosages of applied illumination—$Cd_{1-x}Mn_xTe$ doped with Ga constitutes a unique system for studying carrier-concentration-dependent magnetic effects in semiconductors. In fact, PPC in $Cd_{1-x}Mn_xTe$ has recently been successfully exploited for the observation of electric dipole spin resonance in wide gap DMS's,[9] for the first determination of the magnetization of bound magnetic polarons,[10] and for the study of magnetic-field-induced metal-insulator transition at low temperatures.[11]

Although one of the primary reasons for choosing $Cd_{1-x}Mn_xTe$ for our investigation was to determine whether the photoionization process leading to PPC is itself influenced by a magnetic field, in this study we will focus on the physical mechanism leading to the *generation* of PPC in this material, since the same mechanism should be applicable to a wide range of II-VI's. Specifically, we will show experimental evidence that the strong PPC observed in $Cd_{1-x}Mn_xTe$ doped with Ga is produced by photoionization of a deep defect state related to the Ga dopant. We will develop a two-state model of the defect, and will show that the electron exchange between the ground state of the defect and the conduction band proceeds in two steps, involving an intermediate state which is identified as an optically excited state having the same charge as the ground state. The latter picture is derived from the analysis of photoconductivity transients, based on a two-step photoionization kinetics required to explain our experimental data.

The analysis of our data demonstrates that the number of independent parameters which completely determine the photoionization process can be reduced to *two,* i.e., the two emission rates describing photoexcitation from the ground to the intermediate state, and from the intermediate state to the conduction band. Comparison of the thermal binding energies obtained from Hall measurements and photoionization energies derived from the spectral dependence of the optical cross sections shows that both defect states (the ground and the excited state) are strongly coupled to the lattice, so that the LLR mechanism can be assumed to be responsible for PPC in our material. The defect model developed in this work is very similar to that proposed by Dobaczewski and Kaczor[12,13] for explaining the photoionization kinetics of *DX* centers observed in $Al_xGa_{1-x}As$.

The structure of this paper is as follows. Section II contains a brief review of PPC in II-VI semiconductors and of the physical models proposed over the years to explain this effect. In Sec. III we describe the experimental procedures used in the present study. The experimental results are presented in Sec. IV. In particular, in Sec. IV A we analyze the results of the Hall-effect measurements, and in Sec. IV B we present the photoconductivity transient results, along with the two-step photoionization model which was developed to interpret the data. In Sec. IV C we analyze the spectral dependence of the optical cross sections, and in Sec. IV D we briefly discuss the photoionization experiments carried out in high magnetic fields. Section V presents a summary of our experimental findings and their interpretation.

II. BACKGROUND: PPC IN II-VI SEMICONDUCTORS

Although the PPC effect has been extensively studied in III-V materials, its understanding in II-VI semiconductors is still at a very early stage. In the initial study of wide-gap Cd-based II-VI's, Lorenz and co-workers[14,15] observed a double acceptor center in Cd-annealed *undoped* CdTe, characterized by extremely long recombination times. The authors claimed that upon illumination at low temperatures, one of the electrons bound to the acceptor is excited to the conduction band, making the center singly negatively charged. The Coulomb barrier surrounding the center effectively repels band electrons, thus increasing the recombination time.

Although Losee *et al.*[16] suggested that the observed slow kinetics of the electron transfer in CdTe:Ga cannot be satisfactorily explained by any purely electronic photoexcitation mechanism, in subsequent papers of this group the authors also attributed the PPC behavior in Cl-doped $Cd_{1-x}Zn_xTe$ alloys to the double acceptor model originally proposed by Lorenz.[17,18]

Electron transfer processes with long relaxation times were also observed in *n*-type CdTe heavily doped with Ga, In, Cl, and Br by Iseler *et al.*,[19] who proposed a band-structure-related mechanism for the metastability of the electron states. Specifically, it was noted that the variation with pressure of the donor levels introduced by the above dopants was similar to the pressure dependence of the energy difference between the X minimum and the Γ minimum. This led the authors to associate the donor levels with the conduction-band minima at the X point of the Brillouin zone. The symmetry difference of the wave functions at the Γ and at the X points thus forbids transitions from the Γ minimum to the defect level, explaining the observed extremely long recombination times. However, the electrons can be transferred from the Γ minimum to the X minimum by increasing the temperature, and from there they can fall back into the defect states, thus quenching the PPC.

The role of the coupling between the electronic state of the defect and the crystal lattice in II-VI semiconductors was first experimentally demonstrated by Baj *et al.*[20] These authors explained the pressure-induced changes of the electron concentration in CdTe:Cl by assuming that the donor ions (or other defect centers from which the electron states originate), can alternatively occupy two

nonequivalent positions in the lattice. The two positions of the ions are separated by a potential barrier, and a different electron level is associated with each position. In addition to the electronic transitions between the localized states and the conduction band, the model also allows the donors to be transferred between their two inequivalent lattice positions. Such transfer of donors through the potential barrier can be thermally activated. The slow kinetics of the donor transfer between these two positions separated by a barrier, with a simultaneous change in their charge state, leads to the experimentally observed time dependences of the free-electron concentration. The authors suggest that this model (originally proposed by Porowski, Kończykowski, and Chroboczek[21] to explain transport properties of InSb under hydrostatic pressure) can also be applied to CdTe doped with Ga, Br, or In.

In the past several years, the mechanism involving the interaction of carriers trapped at deep centers with lattice vibrations (the electron-phonon interaction) gained strong experimental support, and is now considered as the main origin of the PPC in II-VI compounds.[22–25] It was recently demonstrated, however, that there exists another mechanism which can lead to PPC in wide-gap II-VI's semiconductors. In *undoped* ternary $Cd_{0.7}Zn_{0.3}Se$ and $CdSe_{0.5}S_{0.5}$ alloys at high temperatures (above 70 K) Jiang and Lin[26–28] attributed the observed PPC to a separation of the photoexcited carriers by electric fields arising from local potential fluctuations caused by compositional inhomogeneities. The model proposed by Jiang and Lin is included here for completeness, but it should be noted that the alloy systems investigated by these authors are qualitatively different from the highly doped and strongly compensated materials described in the preceding paragraphs, which are also the subject of the present study. Thus, the PPC mechanism ascribed to sample inhomogeneities occurring in undoped samples does not contradict the defect-related models commonly applied to PPC in doped materials.

III. EXPERIMENT

In this paper we report an experimental study of PPC performed on n-type $Cd_{0.97}Mn_{0.03}Te$ crystals doped with Ga. The material was prepared in single-crystal form by the vertical Bridgman method, using a high doping level, of the order of 10^{19} cm^{-3}. The samples were cut from the single-crystal ingot in the form of bars with typical dimensions of $4\times2\times0.4$ mm. Six contacts were made to each bar in the Hall configuration, using indium solder. The contacts were Ohmic up to a bias voltage of $V=300$ mV in the entire temperature range of interest ($4\text{ K}<T<300\text{ K}$). The samples were mounted on a copper sample holder in a variable-temperature continuous flow helium cryostat. The sample holder was covered with a thin insulating film, with care taken to ensure good thermal contact, while avoiding electrical contact between the sample and the cryostat.

Two separate experiments were performed. First, Hall-effect measurements were carried out in a weak magnetic field ($B=0.35$ T), in the temperature range from $T=40$ K to $T=300$ K. The data were taken by a computer-controlled data acquisition system, using a constant-current source. The resistivity range of the system was 10^{-2}–10^{10} Ω. The current was automatically adjusted to keep the voltage drop across the sample lower than $V=100$ mV. The proportionality between the measured voltage and the current was checked before measurements at the lowest temperature, to ensure Ohmic behavior of the contacts and to avoid the self-heating of the sample. The main source of uncertainty in the transport data was the finite size of the contacts, which made the distance between the voltage probes uncertain to about 20%.

The Hall-effect measurements were made in two separate temperature runs. For both runs the sample was first slowly cooled down in darkness, with no current passing through it. The cooling process from room temperature to $T=10$ K lasted for many hours (typically ~5 h). The resistivity and the Hall voltage were then measured while the temperature was slowly increased. In the first run the sample was kept in darkness all the time. In the second run, the sample was exposed to illumination at low temperature before starting the warming. The illumination was carried out with white light for about 30 min, until the carrier concentration reached its saturation value (i.e., until all centers were depopulated). The illumination was then switched off, and the measurements were performed as a function of increasing temperature. For both runs, the warming rate was kept at approximately the same value of 2 K/min in the temperature range between $T=25$ and 140 K.

The second experiment consisted of measuring the photoionization cross sections. We used the same setup as that described above, but now the illumination of the sample was by monochromatic rather than white light. To accomplish this, our cryostat was used in conjunction with a 100-W quartz halogen lamp and a 0.22-m, $F/3.9$ grating monochromator. Colored glass band-pass filters in the region 650–1500 nm were used to cut off any second-order radiation. The power of the incident light at each wavelength was measured with a pyroelectric detector and a lock-in amplifier. The output photon flux, of the order of 10^{16} photons/cm^2 sec, was kept constant at each wavelength with a variable attenuator in the visible region, and with calibrated neutral density filters in the infrared region. A concave mirror focused the light onto the sample, with the area of the focal spot slightly larger than the area of the sample. The system beyond the output of the monochromator was enclosed in a specially constructed aluminum enclosure to prevent stray background light from reaching the sample. During the experiment, the sample was slowly cooled down to the desired temperature in darkness, in the time of the order of 5 h. After the temperature was stabilized (with the accuracy of 0.1 K), the monochromatic illumination of the sample was switched on and the measurements begun. The increase of the photoconductivity was measured as a function of time by the same data-acquisition system as in the Hall measurements. After the measurement, the initial conditions were reestablished by heating the system to $T=140$ K in order to quench the PPC.

Measurements of the photoionization cross sections were also carried out in the presence of a strong external magnetic field. The same electronic and optical setups were used, and a similar experimental procedure was followed, but now the sample was placed in an optical cryostat containing a 6-T superconducting magnet.

IV. RESULTS AND DISCUSSION

A. Hall-effect measurements

Typical transport data obtained on our samples are plotted in Fig. 1 as a function of inverse temperature. The triangles correspond to measurements taken before, and the squares after the illumination with white light at low temperatures. The resistivity data shown in Fig. 1(a) clearly demonstrate the strong PPC effect in $Cd_{1-x}Mn_xTe$:Ga. In the temperature range between $T=50$ K and room temperature, the dark resistivity is seen to change by four orders of magnitude. The illumination at low temperatures significantly decreases the resistivity, making the conductivity easily measurable even at low temperatures. As long as the sample temperature is kept below $T=60$ K, the resistivity remains unchanged for many hours after termination of the illumination.

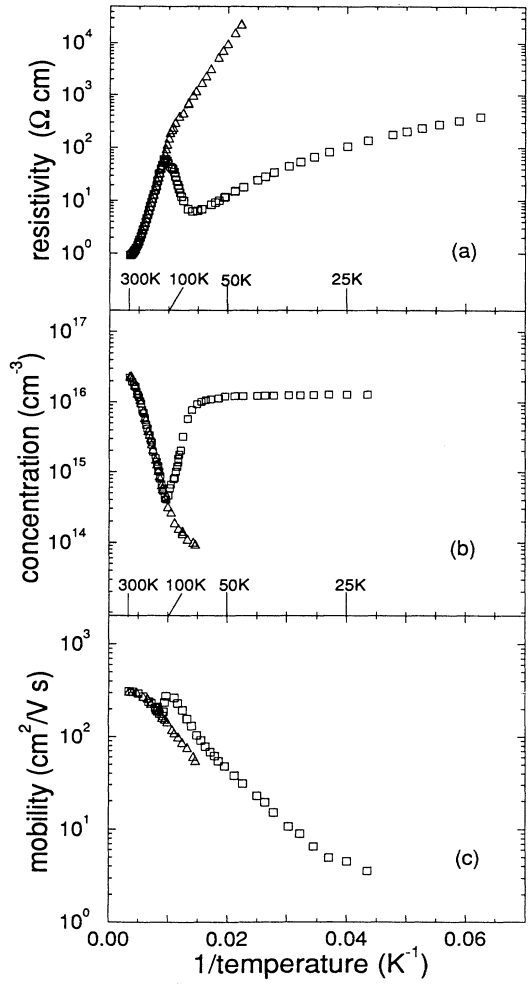

FIG. 1. Dependence of the resistivity (a), Hall concentration (b), and mobility (c) on inverse temperature in Ga-doped $Cd_{0.97}Mn_{0.03}Te$. Triangles and squares denote data taken during a slow warming in darkness and after exposing the sample to light at low temperatures, respectively.

The apparent Hall concentration, derived using the relation $n_H=-1/(eR_H)$, is plotted in Fig. 1(b) as a function of inverse temperature. As the sample temperature decreases in darkness from room temperature, the carrier concentration decreases due to freeze-out of the electrons on the donor level, with a relatively large thermal ionization energy. The donor level occupation equilibrates rapidly (on the time scale of the measurements) and no persistent effect is observed. In order to calculate the thermal ionization energy of the donor level, we consider the standard equilibrium Fermi-Dirac statistics, assuming that only electrons from the Γ-point minimum of the conduction band contribute to the transport. We note from Fig. 1(b) that n exhibits a nearly linear temperature dependence between ~ 80 and ~300 K.

The effective density of states in the conduction band is given by

$$N_c=2\left[\frac{2\pi m_c^* k_B T}{h^2}\right]^{3/2}. \quad (1)$$

Taking $m_c=0.10m_o$ (same as for CdTe), we calculate N_c at $T=80$ and 300 K to be 1×10^{17} cm^{-3} and 8×10^{17} cm^{-3}, respectively. Since the corresponding carrier concentration n changes from 8×10^{15} cm^{-3} to 2×10^{16} cm^{-3} in this temperature region, i.e., $n\ll N_c$, then the carrier concentration n obeys the relation[29]

$$\frac{n(n+N_A)}{N_D-N_A-n}=\frac{N_c}{g_d}\exp\left[-\frac{E_d}{k_B T}\right], \quad (2)$$

where (N_D-N_A) is the net donor concentration (N_D and N_A are the total concentrations of donors and acceptors, respectively), E_d is the thermal activation energy of donors, and g_d is the donor degeneracy factor (equal to 2). Since the concentration of Ga atoms is of the order of 10^{19} cm^{-3} (the technological value of the doping concentration), and the free-electron concentration is only 10^{16} cm^{-3}, the material has to be highly compensated by N_A acceptors, $n\ll N_A<N_D$. This inequality simplifies Eq. (2), and the carrier concentration in the conduction band can then be described by

$$n=n_0\exp\left[-\frac{E_d}{k_B T}\right], \quad (3)$$

where $n_0\equiv(N_D-N_A)N_c/(N_A g_d)$. The nearly linear dependence of the concentration on $1/T$ in the high-temperature region seen in Fig. 1(b) indicates that the factor n_0 remains constant over that temperature range, and the fitting of the data for that region by Eq. (3) yields a thermal activation energy for the donors $E_d=60\pm2$ meV and $n_0=(5.6\pm0.6)\times10^{17}$ cm^{-3}.

In the low-temperature region, below $T=105$ K, the slope of the dark value of n versus $1/T$ changes, and the

electronic equilibrium starts to lag behind the thermal equilibrium. The lag increases as the temperature is lowered, and at sufficiently low temperatures it is impossible to reach electronic equilibrium in a finite time. The relaxation process is so slow that the thermodynamic equilibrium cannot be experimentally obtained, and a metastable value of the electron concentration, higher than the equilibrium concentration, is observed.

Illumination of the sample at low temperatures transfers electrons from the deep traps to the conduction band (from which they can thermalize to shallow states), increasing the carrier concentration by many orders of magnitude (at least two orders at around $T=50$ K and —as can be seen from the trend of the resistivity data— considerably more at low temperatures). At these temperatures the electrons do not have sufficient thermal energy to surmount the capture barrier and to return to their deep levels, thus remaining persistently either in the conduction band or on shallow donors. Warming up the sample in the region $T \leq 60$ K does not affect the carrier concentration n, as can be seen from Fig. 1(b). As the temperature exceeds 60 K, however, the electrons begin to acquire sufficient thermal energy to overcome the barrier, and the free-electron concentration drops rapidly to its equilibrium value.

The corresponding mobility measurements as a function of inverse temperature are shown in the Fig. 1(c), showing data obtained in darkness (triangles) and after illumination (squares). From Fig. 1(c) we can see that the mobility increases with increasing temperature, and its values measured after photoionization, $\mu_{\rm ill}$, remain slightly higher than those measured in darkness, $\mu_{\rm dark}$. As the temperature reaches $T \approx 100$ K, $\mu_{\rm ill}$ suddenly drops and becomes equal to $\mu_{\rm dark}$. Below $T=100$ K the ratio $\mu_{\rm ill}/\mu_{\rm dark}$ is nearly equal to 2. At low temperatures, below 100 K, in highly doped materials the mobility is dominated by ionized impurity scattering. According to the Brooks-Herring theory the mobility should then obey the relation[30]

$$\mu_{\rm ii}=\frac{128\sqrt{2\pi}\epsilon^2(k_BT)^{3/2}}{e^3 m_c^{*1/2} N_I Z^2 \ln(\beta/n)} , \tag{4}$$

where

$$\beta=\frac{96\pi^2 m_c^* \epsilon (k_BT)^2}{e^2 h^2} , \tag{5}$$

and the subscript ii refers to ionized impurity scattering. In the vicinity of 100 K the illumination does not influence the carrier concentration, and according to Eq. (4) the mobility is just inversely proportional to the product of the density of ionized impurities N_I and the square of their charge state Z, $\mu_{\rm ii} \propto 1/(N_I Z^2)$. The observed relation $\mu_{\rm ill}/\mu_{\rm dark} \simeq 2$ can thus be explained by the ionized impurity scattering if we assume that in darkness the scattering centers are doubly charged, and illumination converts them to singly ionized states.[31] The enhancement of mobility after illumination, by approximately a factor of 2, was previously observed also in CdTe:Cl and was regarded as a most convincing evidence for the double-acceptor origin of PPC (Ref. 18) in that material.

B. Measurements of photoionization transients

The large increase of the electron concentration after illumination (by orders of magnitude) in comparison with the corresponding small increase of the mobility (by a factor of 2) allows us to use an approximation where the illumination-induced increase of the conductivity σ is fully attributed to the increase of the free-carrier concentration in the conduction band. Using the above argument and the relation $n=\sigma/(e\mu)$, we will treat the experimentally measured photoconductivity transients simply as the carrier-concentration transients.

Typical results of the carrier-concentration transient measurements at $T=40$ K are shown in Fig. 2. All of the transients, independent of the energy of incident radiation and of temperature, exhibit strongly nonexponential dependence on time and cannot be described by a monoexponential function that would be expected to describe the photoionization process of a single defect. On the other hand, the transients can be very successfully modeled by using a function which is the sum of two exponentials,

$$n(t)=A_1 e^{-e_1 t}+A_2 e^{-e_2 t}+A_3 . \tag{6}$$

The process described by Eq. (6) can be interpreted as a carrier-concentration transient resulting from *independent* photoexcitations of two different defects. According to such an interpretation, e_1 and e_2 represent the photoemission rates of the two independent photoionization processes. The parameter A_3 is then interpreted as the saturation value, and the sum $(A_1+A_2+A_2)$ as the initial value of the carrier concentration in the band.

Although fitting a set of data as smooth as those presented in Fig. 2 with a five-parameter equation is often not particularly meaningful, by a detailed data analysis presented in this section we will show that the number of independent parameters describing the carrier-concentration transients can in fact be reduced to *two*, i.e., the two emission rates e_1 and e_2. Thus the physics of the entire photoionization process is determined

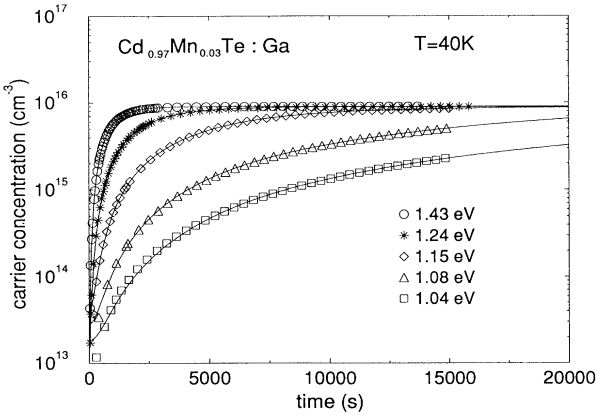

FIG. 2. Carrier-concentration transients in $Cd_{0.97}Mn_{0.03}Te$:Ga at $T=40$ K for different photon energies. Solid curves were calculated by a fitting procedure, based on the two-step photoionization model described in the text [Eq. (16)].

only by the *two* emission rates.

Even preliminary fittings of Eq. (6) to our data lead us to the striking observation that the five parameters are not independent, but appear to be strongly correlated by the relation

$$\left|\frac{A_1}{A_2}\right| = \frac{e_2}{e_1} \ . \tag{7}$$

The above relation was shown to apply at every temperature and photon energy measured. The correlation of these parameters indicates that the processes considered are mutually dependent. The simplest attempt to explain such correlation is to assume that the persistent electrons originate from *one* type of defect, but that the photoionization proceeds in *two* steps. This hypothesis postulates the existence of an intermediate state of the defect, which actively takes part in the carrier exchange between the ground state of the defect and the conduction band (including shallow donor states).

The defect model which we wish to develop for describing our data is very similar to that proposed by Dobaczewski and Kaczor for *DX* centers in $Al_xGa_{1-x}As$.[12,13] A schematic representation of the model is shown in Fig. 3. We assume the presence of N_D shallow donors and N_A shallow acceptors in the material. In the figure N_L and N_U (subscripts L and U refer to the lower and upper state of the same defect, respectively) denote the concentrations of the deep defect states of interest here; and x_L and x_U denote their charge state. If the sample is slowly cooled down in darkness, all of the $(N_D - N_A)$ uncompensated free electrons freeze-out onto the lower defect state. Since every one of the N_L defects can capture x_L electrons, the concentrations of the two states after slow cooling in the dark are

$$N_U = 0 \ , \quad N_L = \frac{1}{x_L}(N_D - N_A) \ . \tag{8}$$

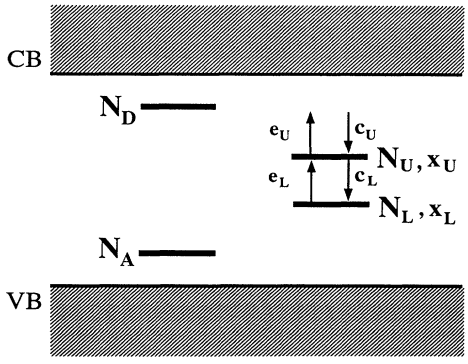

FIG. 3. Diagram illustrating the proposed two-step photoionization of a deep defect responsible for PPC in $Cd_{0.97}Mn_{0.03}Te$:Ga. N_D and N_A denote concentrations of shallow donors and acceptors, respectively. N_L and N_U are concentrations of the defect in the lower state occupied by x_L electrons, and in the upper state occupied by x_U electrons; and $e_{U,L}$ and $c_{U,L}$ represent emission rates and capture cross sections of the two defect states.

The rate equations describing the kinetics of the photoexcitation are given by the following equations:

$$\frac{dN_L}{dt} = -e_L N_L + c_L N_U \ , \tag{9}$$

$$\frac{dN_U}{dt} = -e_U N_U + e_L N_L + c_U(N_D - N_A - N_U - N_L) - c_L N_U \ . \tag{10}$$

Here the emission rates e_U and e_L are the sum of the thermal (e_t) and the optical (e_o) emission rates (where $e_o = \sigma_o \Phi$, σ_o is the photoionization cross section, and Φ is the photon flux), and c_L, and c_U are the capture rates. These capture rates are proportional to the electron concentration in the conduction band, which may result in nonlinearity of the above set of equations. In our case at low temperatures ($T < 60$ K) the capture process is negligibly slow, and can be neglected in comparison to the optical emission. Furthermore, for relatively high photon fluxes used in our measurements ($\Phi \approx 10^{16}$ photons/cm^2 sec), we can neglect the thermal emission as well. Neglecting e_t, c_L, and c_U, the rate equations become linear,

$$\frac{dN_L}{dt} = -e_L N_L \ , \tag{11}$$

$$\frac{dN_U}{dt} = -e_U N_U + e_L N_L \ , \tag{12}$$

and can be solved analytically. The solutions of Eqs. (11) and (12), with the initial conditions given by Eq. (8), are

$$N_L = \frac{1}{x_L}(N_D - N_A)e^{-e_L t} \ , \tag{13}$$

$$N_U = \frac{1}{x_L}(N_D - N_A)\frac{e_L}{e_L - e_U}(e^{-e_U t} - e^{-e_L t}) \ . \tag{14}$$

The electron concentration in the conduction band can be derived from the relation

$$n = (N_D - N_A) - x_U N_U - x_L N_L \ . \tag{15}$$

Taking into account Eqs. (13) and (14), we then obtain an equation describing the transient carrier concentration in the conduction band under illumination:

$$n(t) = (N_D - N_A)\left[\frac{x_U}{x_L}\right]\left[\left[\frac{x_L}{x_U}\right](1 - e^{-e_L t}) - \frac{e_L}{e_L - e_U}(e^{-e_U t} - e^{-e_L t})\right] \ . \tag{16}$$

The solid lines presented in Fig. 2 correspond to the least-squares fit of Eq. (16) to the experimental points. The fitting procedure involves four parameters: the emission rates from the lower and upper levels e_L and e_U, respectively; the ratio of the charge states x_L/x_U; and the parameter $(N_D - N_A)(x_U/x_L)$, which is proportional to the saturation carrier concentration in the conduction band $N_D - N_A$. It should be noted that the fitting curves

presented in Fig. 2 are in remarkably good agreement with the experimental data.

Figure 4(a) summarizes the values of the parameter x_L/x_U obtained from fitting of Eq. (16) to the experimental transients for different photon energies and two different temperatures $T=40$ and 58 K. The most striking feature of this figure is that, within experimental error (which is estimated to be about 5%), the parameter x_L/x_U is independent of the excitation photon energy and is equal to 1. The same result has been obtained for other temperatures below $T=60$ K. Thus, according to our model, the data show that the charge state of the defect center in the lower and upper states is the same.

Using this result ($x_L=x_U$), Eq. (16) can be rewritten in a simpler form,

$$n(t)=(N_D-N_A)\left[1-\frac{e_L}{e_L-e_U}e^{-e_U t}+\frac{e_U}{e_L-e_U}e^{-e_L t}\right], \tag{17}$$

which brings up two important consequences. First, comparison of Eq. (17) to Eq. (6) immediately explains the correlation—mentioned at the beginning of this section—that the ratio of the amplitudes of the two exponential functions equals the ratio of their exponents e_L/e_U [Eq. (7)]. Second, Eq. (17)—in contrast to Eq. (16)—is symmetric with respect to the parameters e_U and e_L, which makes it impossible to recognize which of the two emission rates is related to emission from the lower defect state, and which from the upper level.

Figure 4(b) shows the values of the parameter $(N_D-N_A)(x_U/x_L)$, again for 40 K and 58 K. By taking into account that $x_U/x_L=1$, the above parameter simply denotes the saturation value of the carrier concentration

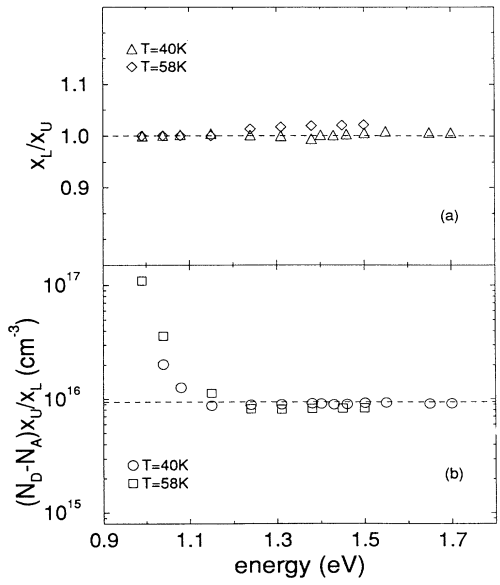

FIG. 4. The parameters x_L/x_U (a) and $(N_D-N_A)(x_U/x_L)$ (b), resulting from the fitting of Eq. (16) to the carrier-concentration transients at $T=40$ and 58 K for various photon energies. The broken lines are a guide for the eye.

in the conduction band. As would be expected, its value is independent of the excitation energy over a wide energy region. For low photon energies, however, the time needed to reach saturation is very long, so that the error of the saturation concentration caused by the finite measurement time is significant. In our opinion, this is responsible for the deviation observed for photon energies lower than 1.1 eV from the constant value in Fig. 4(b). Taking from Fig. 1(c) the mobility values of 23 cm^2/V sec and 68 cm^2/V sec at 40 and 58 K, respectively, the saturation values of the photoconductivity obtained from our measurements provide the following saturation values of electron concentration: $n=0.92\times10^{16}$ cm^{-3} for 40 K, and $n=0.84\times10^{16}$ cm^{-3} for 58 K. These values are in excellent agreement with the carrier concentrations obtained from the Hall measurements, $n_{H\text{ill}}=1.05\times10^{16}$ cm^{-3} [Fig. 1(b)] for $T<60$ K. This agreement between data obtained by two independent measurements provides very strong support for the model.

It should be emphasized that as a result of the above analysis, the number of independent parameters of the photoionization model is *reduced to two,* i.e., the process is completely described only by the emission rates from the upper and the lower states of the defect e_U and e_L. Substituting $x_L/x_U=1$ and $N_D-N_A=n_{H_{\text{ill}}}$ in Eq. (16) results in curves which are very close to those shown in Fig. 2. The emission rates e_U and e_L obtained from the two- and the four-parameter fitting differ by less than a factor of 2. Taking into consideration the strong energy dependence of those parameters discussed in the next section, this argues in favor of the two-parameter procedure.

In order to emphasize the physical meaningfulness of the numerical analysis presented in this section, we point out that the relations $x_U=x_L$ and $N_D-N_A=n_{H_{\text{ill}}}$ were not postulated *a priori,* but were consistently forced upon us by the process of data analysis, starting from the most general case of Eq. (6). These relations may thus be regarded as established by experiment.

C. Optical cross sections

As already remarked, for $x_U=x_L$ it is impossible to determine from Eq. (17) which of the two emission rate values obtained by the fitting, e_U or e_L, is associated with emission from the upper and which from the lower state of the defect responsible for PPC. We will thus change the notation from $e_{U,L}$ to $e_{1,2}$, without specifying which symbol is attributed to which state.

The emission rates $e_{1,2}$ obtained by fitting Eq. (16) to the carrier-concentration transients can also yield the values of the optical cross sections for the photoionization processes of electrons, using the relation $\sigma_{o_{1,2}}=e_{1,2}/\Phi$. Before doing this, we first checked for any possible dependence of the optical cross sections on the photon flux Φ by measuring the photoconductivity transients for different photon fluxes at the same energy and at the same temperature $T=40$ K. The results are presented in Fig. 5. The inset shows that both emission rates e_1 and e_2 are proportional to the flux, indicating that the optical cross sections are flux independent. Both

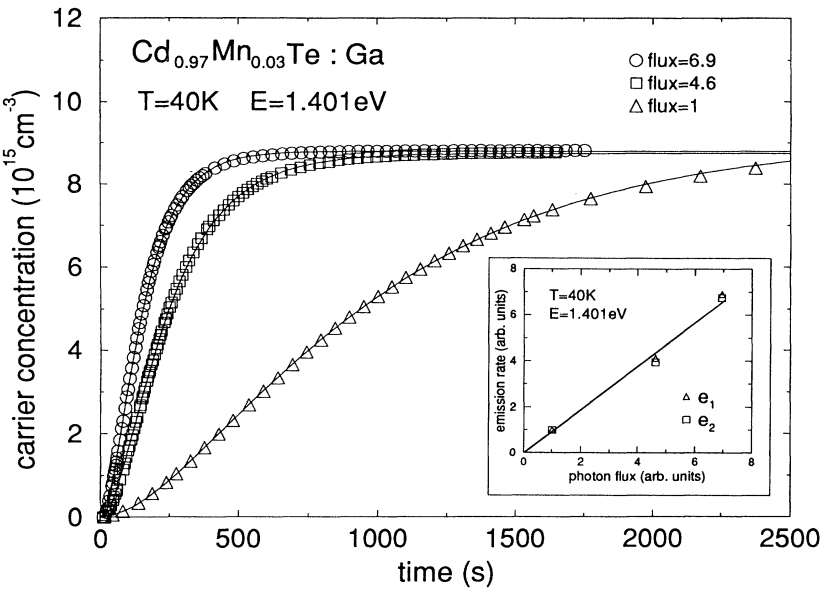

FIG. 5. The carrier-concentration transients at $T=40$ K measured at a fixed photon energy of $E=1.401$ eV for different photon fluxes, and normalized to a flux $\Phi=10^{16}$ photons/cm^2 sec. Solid lines represent the fit of Eq. (16) to the data. The inset shows emission rates e_1 and e_2 resulting from fits as a function of photon flux. The emission rates in the inset are normalized at $\Phi=1$.

σ_{o_1} and σ_{o_2} were normalized at $\Phi=1$ in the inset.

The spectral dependence of the photoionization cross sections σ_{o_1} and σ_{o_2} are shown in Fig. 6 at two temperatures 40 and 58 K. The flattening of the spectra for increasing temperature suggests phonon-induced broadening of the optical transitions. The data were quantitatively analyzed using a model of a localized defect which is strongly coupled to lattice vibrations. For that kind of a system, with a large displacement between the equilibrium positions of the surrounding lattice, the photoionization absorption cross section is given by the relation[4,32]

$$\sigma=\frac{A}{\sqrt{\pi}}\int_{-\beta}^{\infty}dz\, e^{-z^2}\sigma_{\rm el}(E_o\ ,h\nu+E_b z)\left[1+\frac{E_b z}{h\nu}\right]\ , \tag{18}$$

where A is a constant, $h\nu$ is the energy of the incident radiation, E_o is the electronic ionization energy, E_b is the phonon broadening parameter, and β is given by

$$\beta=\frac{h\nu-E_o}{E_b}\ . \tag{19}$$

In the above model the slowly varying part of the optical cross section (corresponding to high photon energies) is mainly governed by the electronic part of the defect wave function. Transitions for very low photon energies (lower than the photoionization threshold E_o), on the other hand, are only possible due to strong electron-phonon interactions. In the above expression the strength of these interactions is described by the broadening parameter E_b, which is highly sensitive to the value of the relaxation energy E_o-E_d and the temperature, and is given by the relation

$$E_b=\left[2(E_o-E_d)\hbar\omega_o\coth\left[\frac{\hbar\omega_o}{2kT}\right]\right]^{1/2}\ . \tag{20}$$

Here $\hbar\omega_o$ is the vibronic energy of the lattice and E_d is the energy of the defect in thermal equilibrium with the conduction band (the donor ionization energy). Huang and Rhys[33] defined an electron-phonon coupling parameter $S=(E_o-E_d)/\hbar\omega_o$ (called briefly the S factor), which gives the average number of phonons emitted as the defect center relaxes after it is optically excited. For convenience, we express the electronic part of the photoionization spectrum $\sigma_{\rm el}(h\nu)$ in terms of a relation proposed by Lucovsky,[34]

$$\sigma_{\rm el}(E_o,h\nu)=A\frac{(h\nu-E_o)^{3/2}}{(h\nu)^3}\ . \tag{21}$$

Table I summarizes the values of the photoionization thresholds E_{o_1} and E_{o_2} and of the broadening parameters E_{b_1} and E_{b_2} resulting from fitting the above model to the observed photoionization rates e_1 and e_2. The solid lines in Fig. 6 are the fitting curves obtained from Eqs.

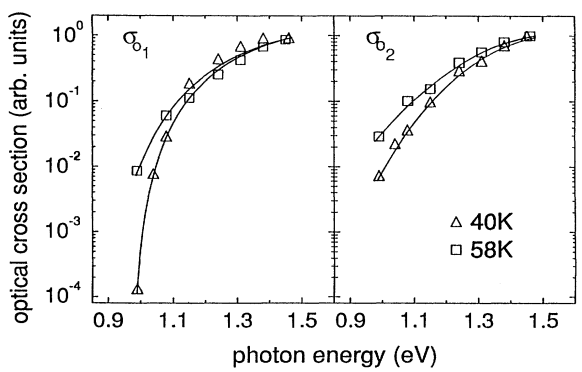

FIG. 6. Photoionization cross sections of the defect states σ_{o_1} and σ_{o_2} at $T=40$ and 58 K. The data are normalized at the photon energy $E=1.48$ eV. Solid lines correspond to the fitting of Eqs. (18)–(21) to the experimental data.

TABLE I. Optical thresholds and broadening parameters at $T=40$ and 58 K obtained from the fitting of Eqs. (18)–(21) to the experimental photoionization cross sections.

T (K)	E_{o_1} (eV)	E_{b_1} (eV)	E_{o_2} (eV)	E_{b_2} (eV)
40	1.09	0.063	0.98	0.050
58	1.10	0.100	1.05	0.098

(18)–(21).

Although we cannot distinguish between emission from the lower and the upper states, the values of the photoionization thresholds $E_{o_{1,2}}$ and broadening parameters $E_{b_{1,2}}$ for both states are very similar (see Table I). For both states the relaxation energies of the lattice are close to 1 eV, and both ionization processes are accompanied by pronounced multiphonon emission. Taking $\hbar\omega_o=0.021$ eV [the longitudinal-optical phonon energy for CdTe (Ref. 35)], the relaxation of the lattice after photoionization of the two states of the defect is accompanied by the emission of $S_1\approx 49$ and $S_2\approx 44$ phonons at 40 K and $S_1\approx 50$ and $S_2\approx 47$ phonons at 58 K, respectively. The high quality of the fit to the experimental data under the assumption of coupling between the defect and the lattice, the pronounced increase of the broadening parameters $E_{b_{1,2}}$ with increasing temperature, and the large difference between the optical and thermal energies (Stokes shifts) all indicate that both states are strongly coupled to the lattice, and that the photoionization of electrons trapped on the defect causes a large lattice relaxation accompanied by phonon emission.

D. Photoionization in the presence of a magnetic field

Although the PPC effect in the wide-gap diluted magnetic semiconductor $Cd_{1-x}Mn_xTe$ has been successfully exploited to study such important topics as the bound magnetic polaron,[10] metal-insulator transition,[11] and electric dipole spin resonance,[9] no attempts have so far been made to address the fundamental question of whether electrons trapped by deep defects in DMS's interact with magnetic spins present in the material. As we already mentioned in the introduction, one of the primary reasons for choosing $Cd_{0.97}Mn_{0.03}Te$:Ga for our investigation was to determine whether the photoionization process leading to PPC is influenced by an external magnetic field, which would be a direct evidence of this type of spin-spin exchange.

The effect of the magnetic field on the electronic properties of DMS's is strongly temperature dependent, and is particularly important at liquid helium temperatures.[8] Unfortunately, with decreasing temperature below $T\approx 40$ K the resistivity of $Cd_{1-x}Mn_xTe$:Ga becomes impossible to measure due to the freeze-out of the free carriers. In order to circumvent this obstacle, in experiments performed at low temperatures ($T=1.5$ K) we preilluminated the sample with a small dose of white light, so as to establish a measurable initial resistivity prior to each experimental run. To check for any possible influence of the preillumination on the photoionization results, we first preilluminated our material at zero magnetic field to reach several initial carrier concentrations from $n=1\times 10^{13}$ cm^{-3} to $n=8\times 10^{14}$ cm^{-3} (assuming the carrier mobility to be $\mu=10$ cm^2/V sec at $T=1.5$ K). Subsequently we measured the photoconductivity and fitted Eq. (17) to the data. None of the four fitting parameters showed any dependence on the initial carrier concentration in this range.

Measurements of the effect of magnetic field on the photoionization process have been done while keeping the initial carrier concentration equal to $n=2\times 10^{13}$ cm^{-3}. We applied several magnetic fields, up to $B=6$ T. The measurements were carried out according to two procedures. In the first, after cooling the sample, allowing the temperature to stabilize, and preillumination, the magnetic field was set at a desired value, and the photoionization measurements were carried out as described in Sec. III. In the second procedure the magnetic field was set before cooling (when the sample was at $T=140$ K), so that the sample was cooled in the presence of the field.

The photoconductivity transients showed no measurable effect of the magnetic field. The parameters comprising Eq. (16) are thus independent of magnetic field (within experimental error), indicating that the photoionization process which leads to PPC in $Cd_{1-x}Mn_xTe$:Ga is, within our experimental error, insensitive to magnetic field. This leads us to conclude that in contrast to shallow levels in DMS's, the deep defect states are not affected, or are very weakly affected by the presence of the Mn^{2+} ions in the lattice.

V. CONCLUSIONS

In the preceding sections we have presented a systematic study of persistent photoconductivity in n-type Ga-doped $Cd_{0.97}Mn_{0.03}Te$. A result of this investigation is that the observed photoconductivity transients exhibit a strongly nonexponential time dependence. A detailed analysis of the transients indicates that the photoionization process leading to PPC can be successfully described by a sum of two mutually dependent exponential functions. This in turn indicates that the carrier exchange between the defect and the conduction band proceeds in two steps via an intermediate state of the defect. Our analysis of the photoexcitation kinetics leads us to identify the intermediate state as an optically excited state having the same charge state as the ground state. We show that the number of independent physical parameters which completely determine the observed photoionization can be reduced to *two*, i.e., the two emission rates describing photoexcitation from the ground state of the defect to the excited (i.e., the intermediate) state and from the excited state to the conduction band.

The spectral and temperature dependence of the photoionization cross sections provide clear evidence that both defect states are strongly coupled to lattice vibrations,

and the large lattice relaxation mechanism is recognized as responsible for PPC in our material. From this point of view the Ga-related defects responsible for PPC in $Cd_{1-x}Mn_xTe$ can be considered as the analogs of *DX* centers in $Al_xGa_{1-x}As$. More experimental and theoretical work, however, remains to be done to determine the microscopic origin of the observed PPC.

ACKNOWLEDGMENTS

We thank Ursula Debska-Bindley and I. Miotkowski for growing the $Cd_{1-x}Mn_xTe$ crystals. The work was supported by the National Science Foundation Grant No. DMR 8913706 and the office of Naval Research Grant No. N00014-90-J-1782.

*On leave from the Institute of Physics, Polish Academy of Sciences, 02-668 Warsaw, Poland.

[1]H. J. Queisser and D. E. Theodorou, Phys. Rev. B **33**, 4027 (1986).
[2]H. J. Queisser, Phys. Rev. Lett. **54**, 234 (1985).
[3]D. V. Lang and R. A. Logan, Phys. Rev. Lett. **39**, 635 (1977).
[4]D. V. Lang, R. A. Logan, and M. Jaros, Phys. Rev. B **19**, 1015 (1979).
[5]For a review, see articles in *Physics of DX Centers in GaAs and Alloys,* edited by J. C. Bourgoin, Solid State Phenomena Vol. 10 (Sci Tech, Vaduz, 1990).
[6]D. J. Chadi and K. J. Chang, Phys. Rev. Lett. **61**, 873 (1988).
[7]D. J. Chadi and K. J. Chang, Phys. Rev. B **39**, 10 063 (1989).
[8]For a review, see *Semiconductors and Semimetals,* edited by J. K. Furdyna and J. Kossut (Academic, Boston, 1988), Vol. 25.
[9]T. Wojtowicz, N. Semaltianos, P. Klosowski, M. Dobrowolska, and J. K. Furdyna, Acta Phys. Pol. **80**, 287 (1991).
[10]T. Wojtowicz, S. Kolesnik, I. Miotkowski, and J. K. Furdyna, Acta Phys. Pol. **82**, 637 (1992).
[11]I. Terry, T. Penny, S. von Molnar, J. M. Rigotty, and P. Becla, Solid State Commun. **84**, 235 (1992).
[12]L. Dobaczewski and P. Kaczor, Phys. Rev. Lett. **66**, 68 (1991).
[13]L. Dobaczewski and P. Kaczor, Phys. Rev. B **44**, 8621 (1991).
[14]M. R. Lorenz and H. H. Woodbury, Phys. Rev. Lett. **6**, 215 (1963).
[15]M. R. Lorenz, B. Segall, and H. H. Woodbury, Phys. Rev. **134**, A751 (1964).
[16]D. L. Losee, R. P. Khosla, D. K. Ranadive, and F. T. J. Smith, Solid State Commun. **13**, 819 (1973).
[17]R. P. Khosla, B. C. Burkey, J. R. Fischer, and D. L. Losee, Solid State Commun. **15**, 1809 (1974).
[18]B. C. Burkey, R. P. Khosla, J. R. Fischer, and D. L. Losee, J. Appl. Phys. **47**, 1095 (1976).
[19]G. W. Iseler, J. A. Kafalas, A. J. Strauss, H. F. Macmillan, and R. H. Bube, Solid State Commun. **10**, 619 (1972).
[20]M. Baj, L. Dmowski, M. Kończykowski, and S. Porowski, Phys. Status Solidi A **33**, 421 (1976).
[21]S. Porowski, M. Kończykowski, and J. Chroboczek, Phys. Status Solidi A **63**, 291 (1974).
[22]R. Legros, Y. Marfaing, and R. Triboulet, J. Phys. Chem. Solids **39**, 79 (1978).
[23]T. Takebe, J. Saraie, and H. Matsunami, J. Appl. Phys. **53**, 457 (1982).
[24]F. Debbag, G. Bastide, and M. Rouzeyre, Solid State Commun. **67**, 1 (1988).
[25]K. Khachaturyan, M. Kamińska, and E. R. Weber, Phys. Rev. B **40**, 6304 (1989).
[26]H. X. Jiang and J. Y. Lin, Phys. Rev. Lett. **64**, 2547 (1990).
[27]H. X. Jiang and J. Y. Lin, Phys. Rev. B **40**, 10 025 (1989).
[28]J. Y. Lin and H. X. Jiang, Phys. Rev. B **41**, 5178 (1990).
[29]S. Blakemore, *Semiconductor Statistics* (Pergamon, New York, 1962).
[30]R. A. Smith, *Semiconductors,* 2nd ed. (Cambridge University Press, Cambridge, England, 1978).
[31]B. Segall, M. R. Lorenz, and R. E. Halsted, Phys. Rev. **129**, 2471 (1963).
[32]M. Jaros, Phys. Rev. B **16**, 3694 (1977).
[33]K. Huang and A. Rhys, Proc. R. Soc. London Ser. A **204**, 406 (1950).
[34]G. Lucovsky, Solid State Commun. **3**, 299 (1965).
[35]K. Zanio, in *Semiconductors and Semimetals,* edited by R. K. Willardson and A. C. Beer (Academic, New York, 1978), Vol. 33.